Prepared for submission to JHEP

A Diffraction Grating for the Cosmic Neutrino Background and Dark Matter

A. Arvanitaki[a] **, and S. Dimopoulos**[a,b]

[a] *Perimeter Institute for Theoretical Physics, Waterloo, ON, Canada*
[b] *Stanford University, Stanford, CA, USA*

E-mail: aarvanitaki@perimeterinstitute.ca, savas@stanford.edu

Abstract: We propose structures of size between ~ 1 meter to 100 meters that drastically alter the local distribution of the Cosmic Neutrino Background ($C\nu B$). These structures have a shape reminiscent of a sea urchin: They consist of rods of width w and length $L \gg w$ periodically arranged on the surface of sphere of radius $R \sim L$. Such a structure functions as a diffraction phase grating and produces a region around its center where the fractional neutrino-antineutrino asymmetry is $\sim k\delta_\nu L$, where k is the neutrino momentum, and δ_ν the deviation of the neutrino index of refraction from unity. The asymmetry has a gradient set by the rod width.

We find that the local neutrino asymmetry can be enhanced by $\mathcal{O}(\text{few} \times 10^6)$ relative to the naive Standard Model expectation, for reasonably sized structures. This results in a force $\mathcal{O}(10^3)$ times bigger than the one we recently pointed out due to the neutrinos' reflection on the surface of the Earth. While in this paper we do not propose a concrete detection setup, we estimate that the $\mathcal{O}(G_F)$ force on a test mass can be close to the Standard Quantum Limit of a torsion balance or a low frequency harmonic oscillator.

Finally, we show that this $C\nu B$ diffractor can be used as a Dark Matter diffractor. For example, the QCD axion Dark Matter with decay constant f_a around 10^9 GeV can be sufficiently diffracted to produce a gradient force that is up to $\mathcal{O}(10^2)$ times larger than the one from the $C\nu B$.

This is the first setup of this kind and the simplicity of our design suggests that there could be significant improvements that escape us.

Contents

1 Introduction

The Cosmic Neutrino Background ($C\nu B$) is a relic of the pre-BBN era and encodes important information about the early universe and the neutrino flavor sector. If discovered, it will explore the Universe at a time when it was less than about one-second-old, well before the time when the Cosmic Microwave Background was created.

Relic neutrinos experience an effective in-matter potential, U [1, 2]:

$$U = \frac{G_F}{2\sqrt{2}}\rho_{\rm matter} \times \begin{cases} (-)(3Z - A) & \text{for } \nu_e \ (\bar{\nu_e}) \\ (-)(Z - A) & \text{for } \nu_{\mu,\tau} \ (\bar{\nu}_{\mu,\tau}), \end{cases} \tag{1.1}$$

where G_F is Fermi's constant, and $\rho_{\rm matter}$ is the number density of atoms in the material. U produces an index of refraction n_ν for neutrinos that differs from one by an amount δ_ν[1]:

$$n_\nu - 1 \equiv \delta_\nu = -\langle \frac{m_\nu U}{k^2} \rangle \tag{1.2}$$

Unfortunately, a "no-go" theorem dating back to 1982 [1, 2] has discouraged a wide class of searches for the $C\nu B$ based on its refractive in-matter effects in the last forty years. This theorem states that since the $C\nu B$ is homogeneous it cannot exert an $\mathcal{O}(G_F)$ refractive force on matter, as it has no preferred direction.

In a recent paper [3], we argued that the presence of matter, such as the Earth, distorts the $C\nu B$ density and causes inhomogeneities that can evade the no-go theorem. In addition,

[1] Electron antineutrinos along with muon and tau neutrinos have an index of refraction larger than unity, while the opposite is true for electron neutrinos together with muon and tau antineutrinos.

	ν_e	$\nu_{\mu,\tau}$
$\lvert\delta_\nu\rvert$ in Water	2×10^{-8}	1.3×10^{-8}
$\lvert\delta_\nu\rvert$ in SiO_2 (rock)	2.5×10^{-8}	2.5×10^{-8}
$\lvert\delta_\nu\rvert$ in Iron	8×10^{-8}	1.1×10^{-7}
$\lvert\delta_\nu\rvert$ in Lead	5.6×10^{-8}	1.9×10^{-7}
$\lvert\delta_\nu\rvert$ in Mercury	7.1×10^{-8}	2.2×10^{-7}
$\lvert\delta_\nu\rvert$ in Gold	1.1×10^{-7}	3.2×10^{-7}
$\lvert\delta_\nu\rvert$ in Tungsten	1.1×10^{-7}	3.1×10^{-7}
$\lvert\delta_\nu\rvert$ in Depleted Uranium	8.2×10^{-8}	3.2×10^{-7}

Table 1. The absolute value of δ_ν for different materials. The neutrino mass is fixed to 0.1 eV.

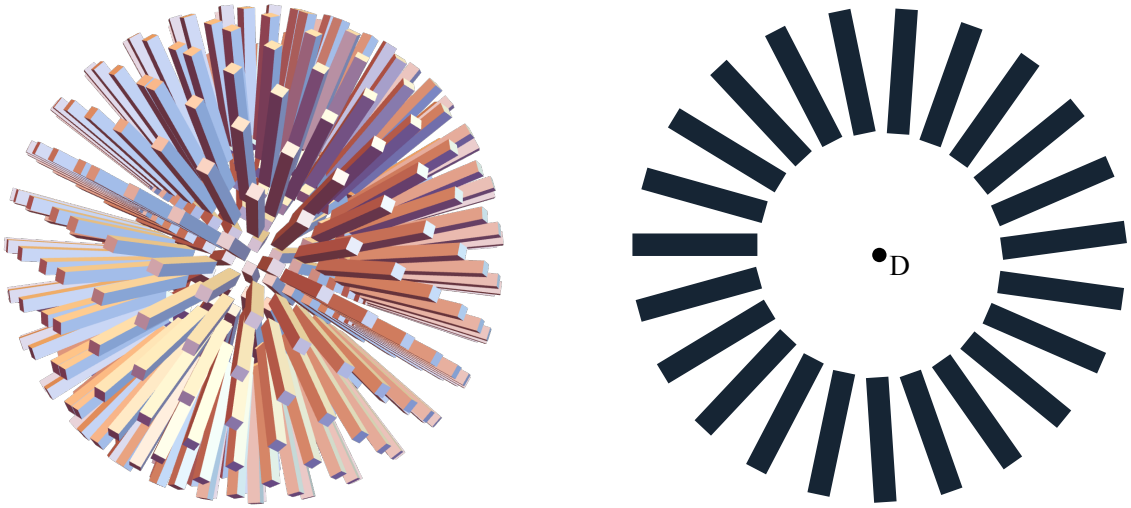

Figure 1. The $C\nu B$ and Dark Matter diffraction phase grating, not drawn to scale. *On the left:* 3D rendering of the grating. Rods of width w and length L are arranged periodically on the surface of a sphere of radius R. *On the right:* 2D slice of the grating that includes the center D of the structure.

since the νs and $\bar{\nu}$s interact differently with matter, the Earth provides a chemical potential that separates them spatially and enhances the local net ν charge density and its gradient, which can directly exert a force on matter. The force from the Earth-induced net neutrino density gradient is many orders of magnitude away from current experiments.

In this paper we factorize the challenge of observing the $C\nu B$ in two parts, manipulation and detection, and address only the first one. This allows us to find an experimental target that we should aim for before the detection of the $C\nu B$ becomes feasible. A rendering of our proposed setup to manipulate the $C\nu B$ is shown in fig. 1. Rods of width w and length L are arranged periodically on the surface of a sphere of radius R.

We show that neutrino waves interact non-trivially with the structure of fig. 1 to produce a $\nu - \bar{\nu}$ asymmetry at its center of size $k|\delta_\nu|L$ and a gradient set by the rod width w. The values δ_ν for different materials are summarized in table 1. We start by showing through the Schrödinger equation that a single rod acts to a good approximation as a

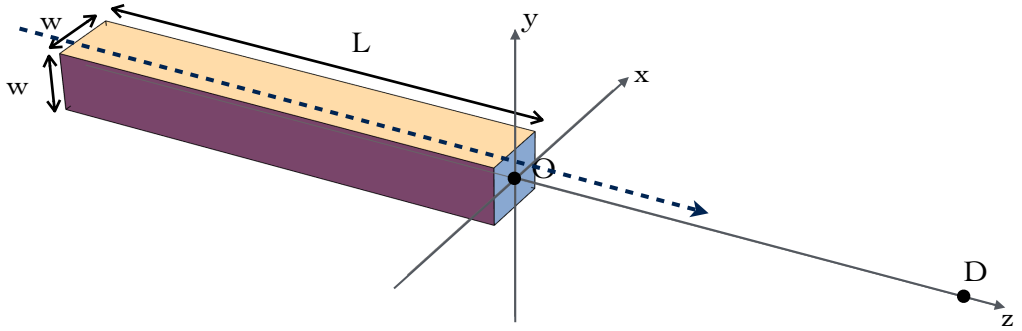

Figure 2. The neutrino diffraction rod of width w and length L. A neutrino and antineutrino wave of momentum k is incident paraxially, and we calculate the fractional asymmetry at point D. For simplicity, we assume that the origin is at point O. The dashed arrow indicates the neutrino wave's direction of propagation for clarity.

phase diffractor for a neutrino wave (see section 2). In section 3, we work out the $\nu - \bar{\nu}$ distribution that a single neutrino rod diffractor produces, and we continue on in section 4 to calculate the $\nu - \bar{\nu}$ distribution induced by the entire structure of fig. 1. We estimate the $\mathcal{O}(G_F)$ force and compare it to the benchmark set by the standard quantum limit (section 5). In section 6 we show that such a structure with appropriate modifications can be used to locally alter the DM density. For the QCD axion, while this change is only a small fraction of its local density, it can produce a refractive force that is 100-1000 times bigger than the one produced by the $C\nu B$. In section 7 we discuss the stochastic $C\nu B$ and axion DM forces due to the local fluctuations in density and we compare them to those produced by the structure of fig. 1. We conclude in section 8.

2 Schrödinger equation for a neutrino wave incident on a rod

In this section we study the Schrödinger equation for a neutrino wave of momentum k incident paraxially on a diffraction rod. The rod is of length L and square cross-section of width w, as shown in fig. 2.

The interaction is described by the stationary Schrödinger equation:

$$\nabla^2\psi_\nu + 2m_\nu(E - U(\vec{x}))\psi_\nu = (\nabla^2 + n^2(\vec{x})k^2)\psi_\nu = 0 \tag{2.1}$$

Here, $U(\vec{x})$ is the interaction potential of the neutrino with matter,and $n(\vec{x})$ is the index of refraction, which is close to unity. We will write it as $n(\vec{x}) = 1 + \delta_\nu(\vec{x})$. We can remove the dominant z-dependence of the solution by going to the rest-frame of the incident neutrino, setting $\psi_\nu = e^{-ikz}\tilde{\psi}_\nu(\vec{x})$ and find [4, 5]:

$$i\frac{\partial\tilde{\psi}_\nu}{\partial z} = k\delta_\nu\tilde{\psi}_\nu + \frac{1}{2k}\nabla^2\tilde{\psi}_\nu \tag{2.2}$$

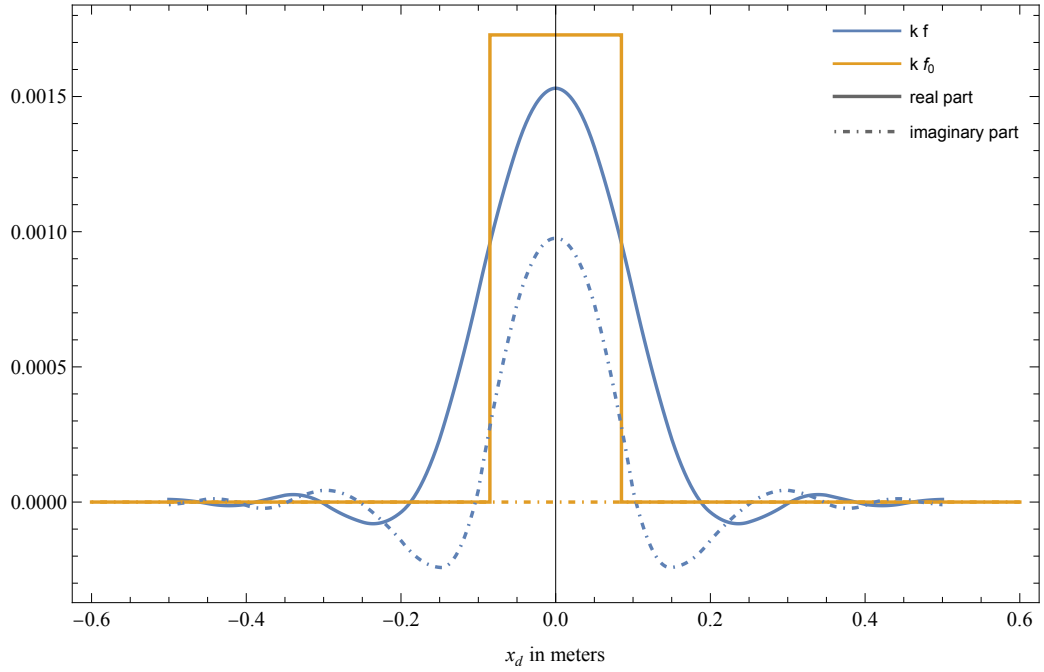

Figure 3. The real (solid blue line) and imaginary (dot-dashed blue line) part of the exact solution $kf(x,z)$ from eq. 2.4 for a paraxial wave with momentum k incident on the rod of fig. 2, and the corresponding first order approximation kf_0 for the same problem (solid and dot-dashed orange lines). The length of the tungsten rod is chosen to be 10 meters with the width of 0.17 m, and we assume an electron antineutrino wave with momentum $k = \frac{2\pi}{0.004\ \mathrm{m}}$.

So, the z-evolution of $\tilde{\psi}_\nu$ obeys the time dependent Schrodinger eqs with z playing the role of time, $k\delta_\nu$ the role of the potential, and k the mass. We are interested in computing the profile of $\tilde{\psi}_\nu(x,y,z=0)$ at $z=0$ from the z-evolution of $\tilde{\psi}_\nu$ from $z=-L$ where $\tilde{\psi}_\nu = 1$. In the geometric optics limit where the effective mass k is large, the second kinetic term on the right hand side can be neglected and the evolution is dominated by the pure potential term:

$$\tilde{\psi}_\nu(x,y,z) = e^{-ik\int_{-L}^{z}\delta_\nu(x,y,z')dz'},\ \text{so that}\ \psi_\nu = e^{-ik\int_{-L}^{z}n(x,y,z')dz'} \tag{2.3}$$

In this eikonal solution the evolution of the phase is proportional to the "optical" path length weighted by the index of refraction. As we will see this will turn out to be a good approximation in our case, to about 10%. To find corrections to this it is convenient to make the ansatz $\tilde{\psi}_\nu = e^{-ikf(x,y,z)}$ in equation 2.2 as inspired by the WKB ansatz. We find:

$$\frac{\partial f}{\partial z} = \delta_\nu - \frac{i}{2k}\nabla^2 f - \frac{1}{2}(\nabla f)^2 \tag{2.4}$$

This is a time dependent WKB eqs where "time" is z and with initial condition $f=0$ at $z=-L$. In the usual WKB case, the non-linear term is dominant because the action kf in the exponent is large. By contrast in our case the kf is small: f starts out zero at $z=-L$ and evolves linearly $f=\delta_\nu(z+L)$ inside the material, when δ_ν is z-independent.

So, unless z is very large f does not grow large and the non-linear term is negligible - this is the opposite of the WKB limit. For the case when the potential is independent of z we can solve for f iteratively starting with $f_0 = \delta_\nu(z+L)$, and we find the first correction f_1 to be:

$$f = f_0 + f_1 = \delta_\nu(z+L) - \frac{i\,(z+L)^2}{4k}\left(\frac{\partial^2\delta_\nu}{\partial x^2} + \frac{\partial^2\delta_\nu}{\partial y^2}\right) \tag{2.5}$$

We can estimate the relative importance of the two terms by replacing the derivative with its coarse grained value $1/w$. The second term is subdominant by $\sim \frac{z}{2kw^2}$. This is $\mathcal{O}(10\%)$ for our parameters. This naive estimate agrees well with the exact numerical solution of eq. 2.4 which is shown in fig. 3. It is worth pointing out that the dispersive term of eq. 2.4 also adds a small imaginary correction to $f_0 = \delta_\nu(z+L)$. For the rod lengths L and widths w considered later in sections 3, and 4, we can safely ignore in our conclusions the dispersive term. In what follows, we will calculate the $\nu - \bar{\nu}$ asymmetry generated by the diffraction grating shown in fig. 1 by just taking into account f_0, i.e. the effective phase of a ray as the wave goes through the material relative to the vacuum. This approach treats our setup as a diffraction phase grating only, and ignores its effects as an amplitude grating, which is caused by the dispersive term.

3 A rod as a neutrino phase diffractor

Before we go on to consider the effect of the full diffraction grating of fig. 1 on the neutrino distribution, it is instructive to work out the corresponding effect of a single diffraction rod. As explained in the previous section, a paraxial neutrino wave of momentum k after it has gone through the rod of fig. 2 is given to a good approximation by:

$$\psi_\nu = e^{-ikz} \times \begin{cases} e^{-ik\delta_\nu L} & \text{for } |x| \le \frac{w}{2} \text{ and } |y| \le \frac{w}{2} \\ 1 & \text{for } |x| \ge \frac{w}{2} \text{ or } |y| \ge \frac{w}{2}, \end{cases} \tag{3.1}$$

i.e. the wave going through the rod differs from a plane wave only by the phase $k\delta_\nu L$ it acquires relative to the vacuum due to its non-trivial path inside the material.

We want to calculate the field at a distance z_d from the position of the rod and its profile at small distances, x_d and y_d, away from the long axis of symmetry of the system, as shown in figure 2. This can be done in using the Kirchhoff integral theorem [6]:

$$\psi_{\nu d} = \frac{ik}{4\pi}\int_{-\infty}^{+\infty}\int_{-\infty}^{+\infty}\left(\psi_\nu \frac{e^{-ikr_d}}{r_d}(\hat{z}\cdot\hat{r_d}+1)\right)dxdy, \tag{3.2}$$

where r_d is the distance of points on the $z=0$ plane from (x_d, y_d, z_d). In the above equation, we can use the small phase approximation, $e^{-ik\delta_\nu L} \approx 1 - ik\delta_\nu L$, and isolate the plane wave component of $\psi_{\nu d}$ to get:

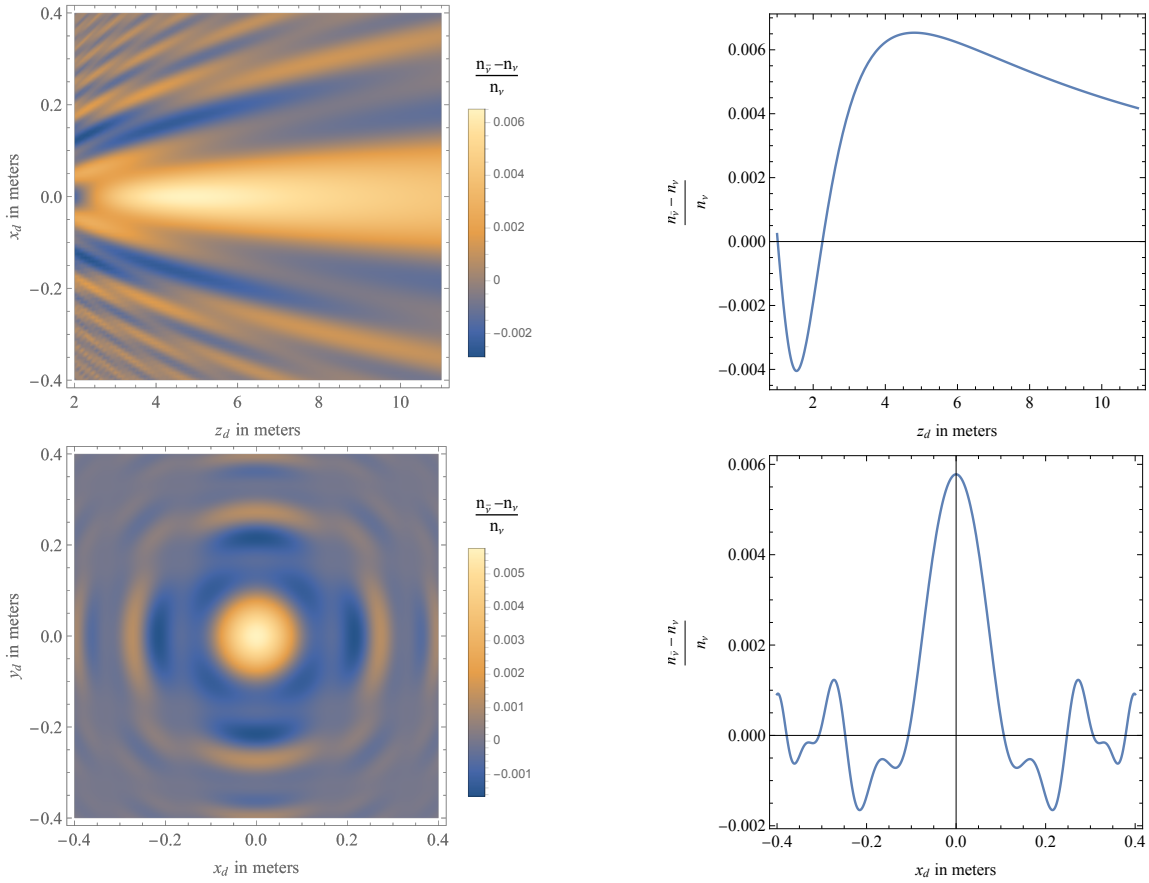

Figure 4. Different profiles of the neutrino asymmetry produced by a electron neutrino and antineutrino wave that are paraxial on the diffraction rod of fig. 2. *Top left:* The neutrino asymmetry as a function of the distance z_d from the face of the rod and the distance x_d from the axis of symmetry (see figure 2 and text for more details). We fix the rod width w to be 17 cm, the rod length is $L = 10$ m, and pick a wavelength of $\lambda = 4$ mm for the neutrino waves. The asymmetry is plotted for an index of refraction corresponding to tungsten. *Top right:* The same asymmetry as a function of the distance z_d from the face of the rod along the axis of symmetry ($x_d = 0$, and $y_d = 0$). *Bottom left:* The same asymmetry as a function of the distance x_d and y_d from the axis of symmetry at $z_d = 7$ m for concreteness.*Bottom right:* The same asymmetry as a function of x_d, fixing $y_d = 0$ and $z_d = 7$ m.

$$\psi_{\nu d} \approx e^{-ikz_d} + \frac{k^2\delta_\nu L}{2\pi}\int_{-\frac{w}{2}}^{+\frac{w}{2}}\int_{-\frac{w}{2}}^{+\frac{w}{2}}\left(\frac{e^{-ikz_d}}{z_d}e^{-ik\frac{(x-x_d)^2}{2z_d}}e^{-ik\frac{(y-y_d)^2}{2z_d}}\right)dxdy, \tag{3.3}$$

where we have set for simplicity the endpoint of the rod at $z = 0$ and taken the limit $|x_d|, |y_d| \ll z_d$. One can easily now identify the integral in the parenthesis as the Kirchhoff integral of a plane wave diffracting from an opening on a dark screen. The neutrino antineutrino asymmetry at point D can now be calculated in this toy model as:

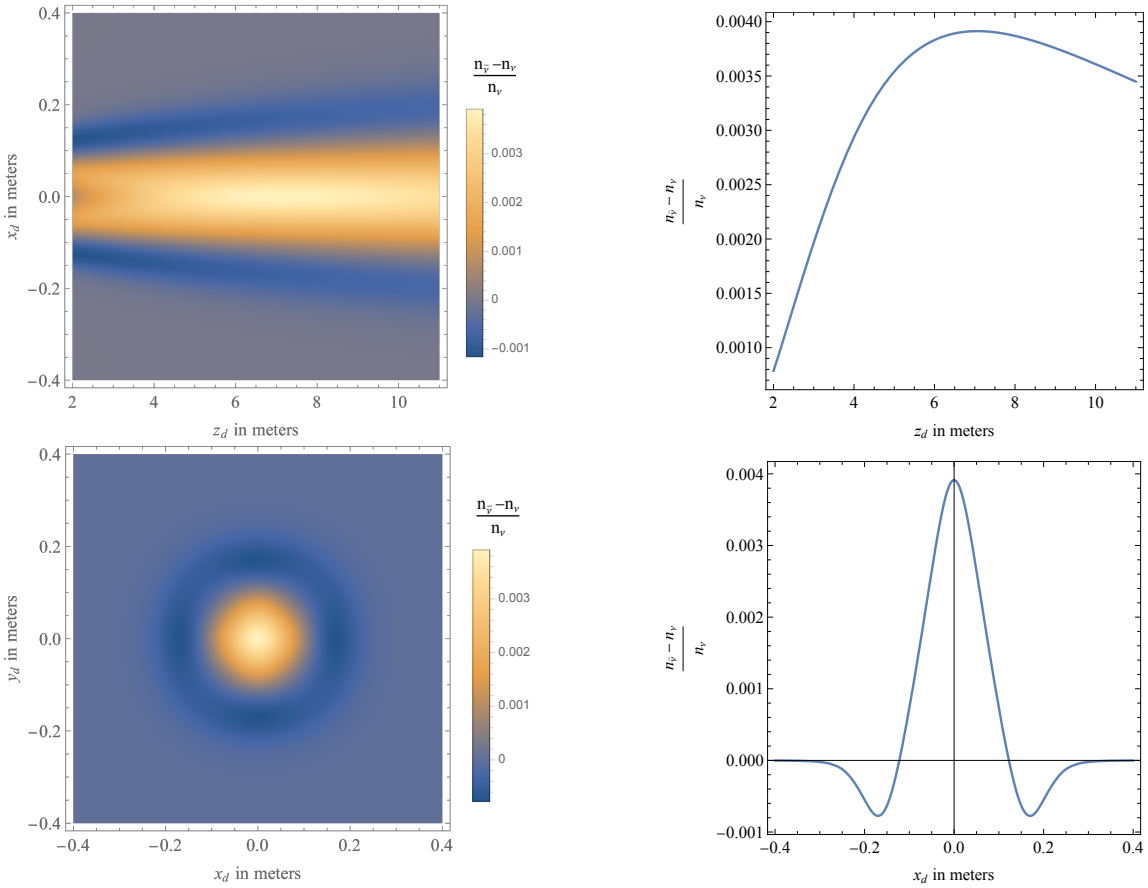

Figure 5. Different profiles of the momentum averaged neutrino asymmetry produced by electron neutrino and antineutrino waves that are paraxial on the diffraction rod of fig. 2. *Top left:* The momentum averaged neutrino asymmetry as a function of the distance z_d from the face of the rod and the distance x_d from the axis of symmetry (see figure 2 and text for more details). We fix the width w to be 17 cm and the length L we set at 10 m. The asymmetry is plotted for an index of refraction corresponding to tungsten. *Top right:* The same asymmetry as a function of the distance z_d setting $x_d = y_d = 0$. *Bottom left:* The same asymmetry as a function of the distance from the axis of symmetry x_d, and y_d. The distance z_d is fixed to 7 m. *Bottom right:* The same asymmetry as a function of x_d alone, with $y_d = 0$ and $z_d = 7$ m.

$$\frac{n_{\bar{\nu}} - n_\nu}{n_\nu}(k) = \left. |\psi_{\nu d}|^2 \right|_{\delta_\nu > 0} - \left. |\psi_{\nu d}|^2 \right|_{\delta_\nu < 0} \approx$$
$$4\ Re\left[\frac{k^2 \delta_\nu L}{2\pi} \int_{-\frac{w}{2}}^{+\frac{w}{2}} \int_{-\frac{w}{2}}^{+\frac{w}{2}} \left(\frac{1}{z_d} e^{-ik\frac{(x-x_d)^2}{2z_d}} e^{-ik\frac{(y-y_d)^2}{2z_d}}\right) dxdy\right], \quad (3.4)$$

and it is plotted in fig. 4. One can see that the asymmetry is maximized right on axis at the point $z_d \sim \frac{w^2}{\lambda}$, where λ is the neutrino wavelength, and it persists in a region of order $x_d \sim w$ before it flips sign. This excess is generated by diffraction; this maximum first appears when all the partial waves from the front of the rod add up coherently. As

expected the maximum value of this asymmetry is of order $k|\delta_\nu|L$. As one moves away from $z_d \sim \frac{w^2}{\lambda}$ the asymmetry pattern spreads as $\sqrt{\lambda z_d}$ just as expected from a diffraction pattern.

The $C\nu B$ is of course neither monochromatic nor collimated. Assuming that the $C\nu B$ follows a unidirectional Fermi-Dirac distribution, the momentum averaged asymmetry is given by:

$$\left.\frac{n_{\bar{\nu}} - n_\nu}{n_\nu}\right|_{\text{average}} = \frac{\int k^2 dk \frac{n_{\bar{\nu}} - n_\nu}{n_\nu}(k)(e^{k/T_\nu}+1)^{-1}}{\int k^2 dk (e^{k/T_\nu}+1)^{-1}} \tag{3.5}$$

The integral in the numerator needs to be cutoff at wavelengths larger than the width of the rod. We conservatively set a maximum neutrino wavelength of 4 cm, for $w = 0.17\ m$. The result of numerically integrating eq. 3.5 is plotted in fig. 5. We find that, in order for the asymmetry and its gradient to be maximized, the optimal parameters of the width of the rod w vs the distance z_d have to be chosen through the relation $z_d \sim \frac{w^2}{\lambda}$ for the expectation value $\langle k^{-1}\rangle = \frac{0.003\ \text{m}}{2\pi}$, or $\lambda_{av} = 3$ mm. At distances larger than the optimal, the asymmetry drops roughly linearly with z_d and the diffraction pattern gets smoothed out as $\sqrt{z}$.

To conclude, a rectangular piece of material is enough to diffract a neutrino wave and create a local fractional excess of neutrinos vs antineutrinos at position $\frac{w^2}{\lambda}$ of size of order $k\delta_\nu L$ and a gradient of size $\sim w$. Due to the diffractive nature of the effect, the qualitative features just described are universal and roughly independent of the shape of the cross-section of the rod, so its engineering does not have to be very precise.

Unfortunately, the neutrinos are not unidirectional, and instead come from all directions. The naive acceptance angle of this rod is of order $\frac{w^2}{(z_d+L)^2}$, which is particularly small for any realistic construction and would suppress the naive asymmetry calculated above. We address this issue in the upcoming section.

4 A compound diffraction grating for the $C\nu B$

The $C\nu B$ is thermal radiation and, as such, it is omnidirectional. An obvious perhaps way to address this issue and create a sizeable neutrino-antineutrino asymmetry is to orient multiple neutrino diffraction rods radially along the surface of a sphere or radius R as shown in fig 1. There is a small gap of w_1 from one rod to the next (see also figures 6 and 7). In this section we will argue that this configuration produces an asymmetry around the center of the structure. The size of the asymmetry is roughly $k\delta_\nu L$ and it has a gradient of order $\mathcal{O}(w)$, after the neutrino distribution is integrated over both momentum and angle.

Our first instinct is to assume that the total asymmetry would be a simple superposition of what is produced by the single diffraction rod presented in the previous section. This is only correct for waves paraxial to the rod. When considering waves that are no longer paraxial, one can see that there is another type of diffractor that can be identified in 1 that includes two rods at an angle of $\frac{w+w_1}{R}$. This is shown more precisely in figure 6. A paraxial

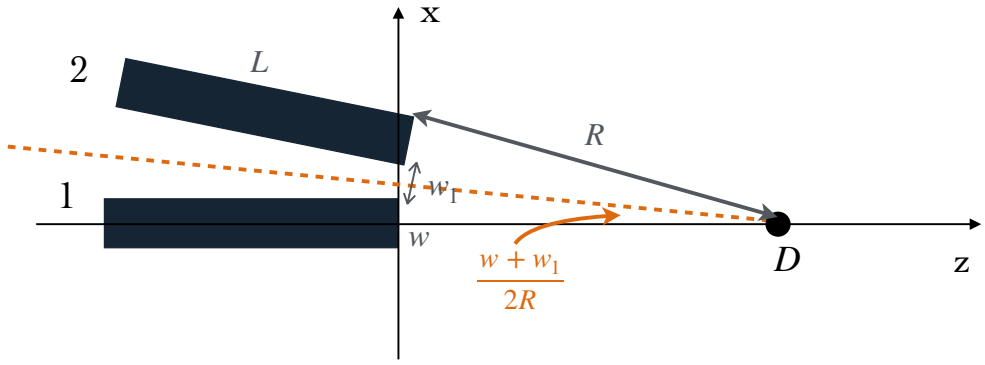

Figure 6. A two rod subsection of the setup shown in fig. 1. Each rod is of width w and length L as in sec. 3. There is a small gap of w_1 between the rods. The angle between the axes of the rods is $\frac{w+w_1}{R}$. The direction of the neutrino wave is indicated by the angle $\theta = \frac{w+w_1}{2R}$.

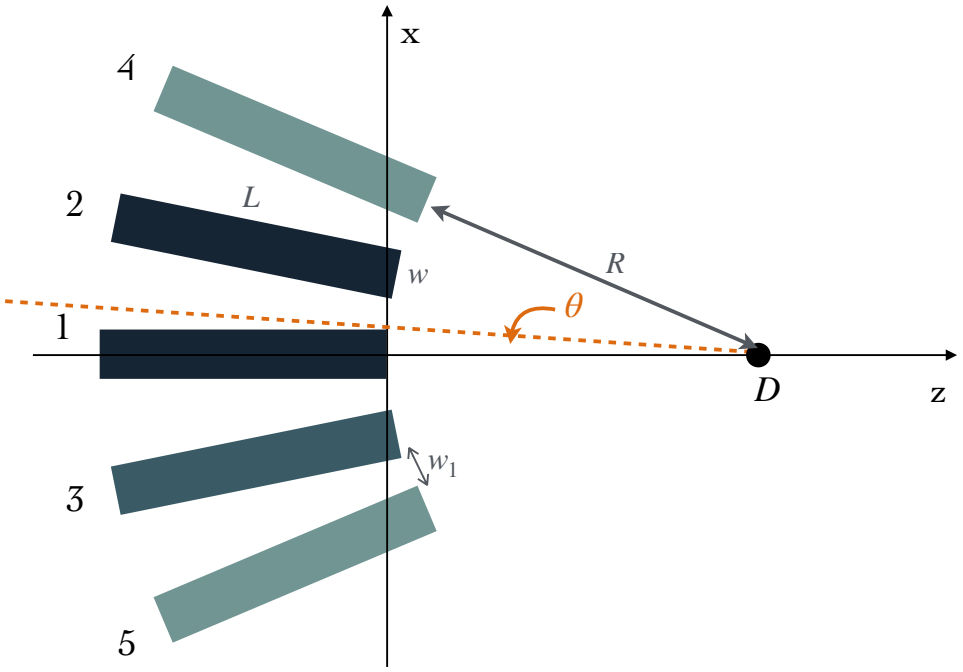

Figure 7. A five rod subsection of the setup shown in fig. 1. Each rod is of width w and length L as in sec. 3. There is a small gap of w_1 between the rods. The angle between the axes of two subsequent rods is $\frac{w+w_1}{R}$. The direction of the neutrino wave is indicated by the angle θ. Different combinations of the numbered rods 1-5 are discussed in the text.

wave on this diffraction configuration will be incident at an angle $\frac{w+w_1}{2R}$ in the $z-x$ plane, right in the middle between the two rods.

Following the procedure described in sec. 3, we can calculate the resulting diffracted wave around the center of this set-up at point D of fig. 6, by first computing the effective optical path length as a function of x. We find the effective optical path as a function of x

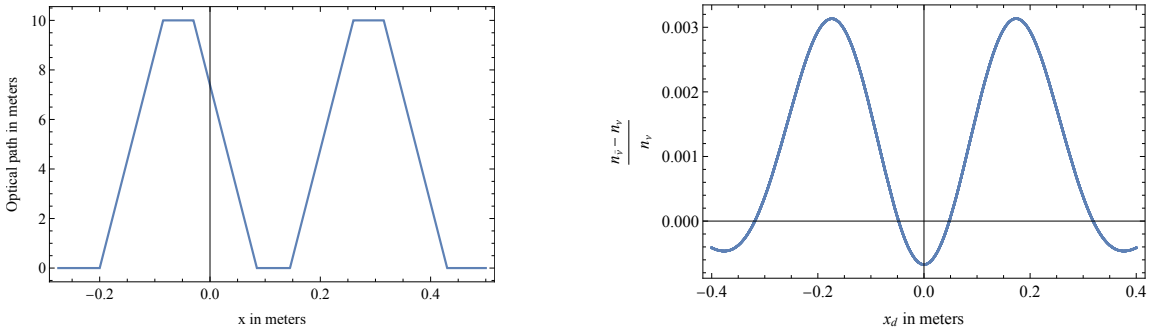

Figure 8. *On the left:* The effective path length of an electron neutrino and antineutrino wave incident right in between rods 1 and 2 shown in figure 6, i.e. $\theta = \frac{w+w_1}{2R}$. *On the right:* The corresponding momentum averaged neutrino assymmetry. For concreteness we have taken $w = 0.17$ meters, $w_1 = 0.06$ meters, and $R = L = 10$ meters. Each rod is made out of tungsten.

that is shown on the left panel of fig. 8.

Taking again the small $k\delta_\nu L$ approximation, the asymmetry produced in the x direction around the center of this configuration at point D is shown on the right panel of figure 8. As perhaps expected, the maximum of the antineutrino excess is shifted to the side, and there is a small neutrino excess now at the center.

The final asymmetry will be calculated by superimposing all of these diffraction gratings. As shown in sec. 3, the asymmetry and the corresponding gradient can be maximized when choosing the radius R of the sphere along which the rods are placed to be related with the width w of each rod by:

$$R \sim \frac{w^2}{\lambda_{av}}, \tag{4.1}$$

where $\lambda_{av} \approx 3$ mm, is the value of the neutrino wavelength that optimizes averaging over momenta, as was calculated in section 3. The length L of each rod needs to be close to R so that the optical path for any incidence angle is maximized. The gradient is further maximized, when we choose $w_1 = \frac{w}{3}$, in order to produce well separated diffraction patterns from each rod without losing in angular coverage. In order for the diffraction patterns from every rod to be optimal, we roughly need to choose $w \sim \sqrt{\lambda_{av} R}$, as calculated at the end of sec. 3. This means that while the asymmetry grows linearly with the size of the structure $L \sim R$, the gradient of that asymmetry scales as $\sqrt{R}$, since $w \propto \sqrt{R}$.

The final asymmetry will be determined by integrating over the neutrino incidence angle. For this we will consider three sets of fiducial parameters for our diffraction grating, which are summarized in table 2. Because the structure of fig. 1 is periodic, we apply Kirchhoff's theorem for a small number of rods in the x direction, as shown in fig. 7. A neutrino wave with an incidence angle $\theta << 1$ on the structure of fig. 7 will result in a wave around the position $z_d = R$ and $y_d = 0$, which in the small θ and $k\delta_\nu L$ approximation is given by:

Set-up parameters	Grating 1	Grating 2	Grating 3
Rod Material	Depleted Uranium	Tungsten	Iron
Rod length L	2 meters	10 meters	100 meters
Rod width w	0.08 meters	0.17 meters	0.54 meters
Inter-rod gap w_1	0.03 meters	0.06 meters	0.18 meters
Grating radius R	2 meters	10 meters	72 meters

Table 2. The sets of parameters for the diffraction grating shown in fig. 1 considered in this section. The profile of the fractional $\nu - \bar{\nu}$ asymmetry for each one is plotted in fig. 10. The neutrino index of refraction for different material is shown in table 1

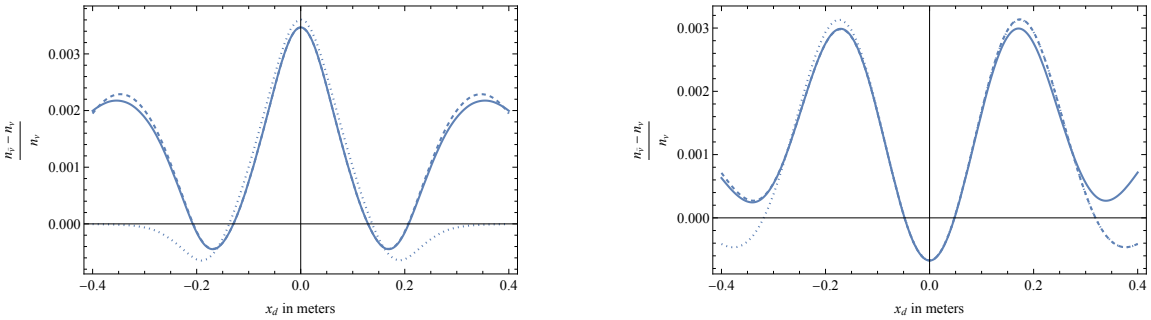

Figure 9. *On the left:* The momentum averaged neutrino asymmetry as a function of the distance x_d from the axis of symmetry for 1 (dotted line), 3 (dashed line), and 5 (solid line) rods (see text for more details). The grating parameters are those of the second setup proposed in table 2, and the neutrino wave is incident on an angle $\theta = 0$. *On the right:* The same asymmetry as a function of the distance x_d for 2 (dotted line), 3 (dashed line) and 5 (solid line) rods with the incidence angle $\frac{w+w_1}{2R}$. Other parameters are the same as above.

$$\psi_{\nu d} \approx e^{-ik\cos\theta R + ik\sin\theta x_d} + \frac{k^2\delta_\nu}{2\pi}\int_{x_{\min}}^{x_{\max}}\int_{-\frac{w}{2}}^{+\frac{w}{2}} e^{ik\sin\theta\ x - ik\cos\theta\frac{x^2+y^2}{2R}} L(\theta,x)\times \left(\frac{e^{-ikR}e^{ik\frac{x^2+y^2}{2R}}}{R} e^{-ik\frac{(x-x_d)^2+y^2}{2R}}\right) dydx. \tag{4.2}$$

In the above equation, the $L(\theta, x)$ is the optical path inside matter, and $x_{\min}(x_{\max})$ denote the appropriate range of x over which the optical path is non-zero. After calculating the effective path for a neutrino wave with a incidence angle $\theta = 0$ for 1, 3 and 5 rods, and $\theta = \frac{w+w_1}{2R}$ for 2, 3 and 5 rods, we present the result in fig. 9 in each case. Fig. 9 shows that a 2-rod configuration captures already the dominant behavior of the setup around the axis of symmetry, while increasing the number of rods from 3 to 5 there is at most $\mathcal{O}(10\%)$ difference for the asymmetry around the center. A five rod segment is thus more than enough to accurately calculate the asymmetry within a radius of size $\sim 2w$ around the center point D of a diffraction grating of size R.

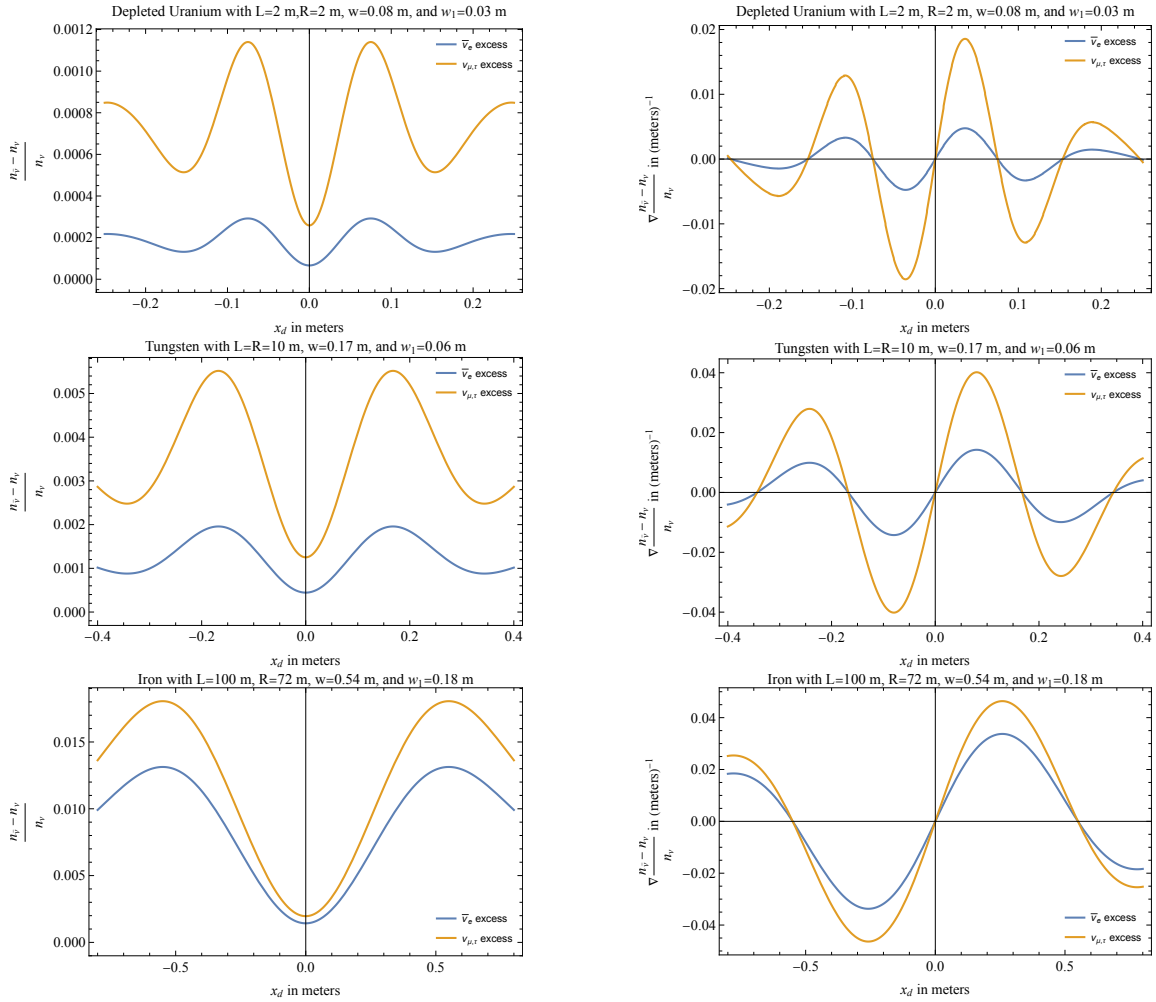

Figure 10. The produced neutrino asymmetry and the corresponding gradient for gratings 1, 2, and 3 summarized in table 2. *Top left: Grating 1* The fractional momentum- and angle-averaged neutrino asymmetry for all neutrino flavors as a function of the distance x_d from the axis of symmetry produced by 5 rods (see fig. 7, and the text for more details). *Top right: Grating 1* The corresponding gradient for the above asymmetry as a function of the distance x_d for 5 (solid line) rods. *Center left: Grating 2* Same as top left plot but for grating 2 parameters. *Center right: Grating 2* Same as top right plot but for grating 2 parameters. *Bottom left: Grating 3* Same as top left plot but for grating 3 parameters. *Bottom right: Grating 3* Same as top right plot but for grating 3 parameters.

Our proposed structure is periodic in the angular direction with an angular period of $\frac{w+w_1}{R}$, so in order to calculate the $C\nu B$ distribution at a region close to the center of our proposed diffraction grating, we just need to average over the neutrino momentum and the incidence angle from $\theta = 0$ to $\theta = \frac{w+w_1}{2R}$:

$$\left.\frac{n_{\bar{\nu}}-n_\nu}{n_\nu}\right|_{\text{average}} = \frac{\int_0^{\frac{w+w_1}{2L}} \int d\theta\ dk\ k^2 \sin\theta\ \frac{n_{\bar{\nu}}-n_\nu}{n_\nu}(k,\theta)(e^{k/T_\nu}+1)^{-1}}{\int_0^{\frac{w+w_1}{2L}} \int d\theta\ dk\ k^2 \sin\theta\ (e^{k/T_\nu}+1)^{-1}} \tag{4.3}$$

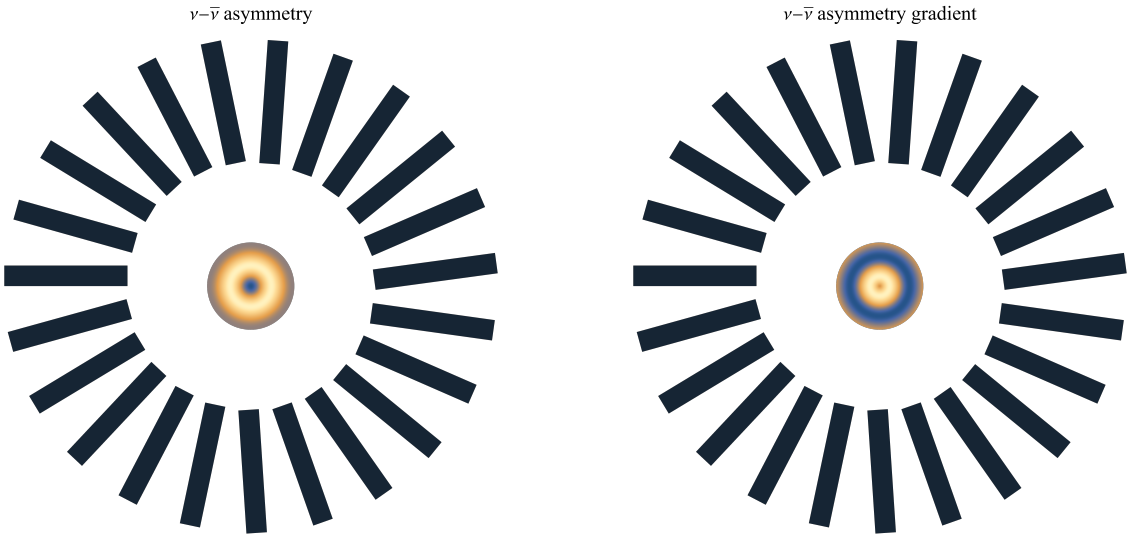

Figure 11. *On the left:* The momentum and angle integrated asymmetry produced around the center of the diffraction grating shown in fig. 1. Brighter spots corresponds to larger positive asymmetry. The asymmetry and the grating are not drawn to scale. *On the right:* The corresponding gradient. Brighter sports correspond to larger positive gradient while darker spots correspond to larger negative gradient. As previously, the gradient and the grating are not drawn to scale.

As in sec. 3, this integral is cutoff at large neutrino wavelengths, which for our case is set to 4 cm. This integral also assumes a cylindrical symmetry around the axis of the central rod No. 1 of fig. 7. This clearly is not true for our full proposed setup of 1. Nevertheless, we expect that our approximation should be true to a factor of $\mathcal{O}(1)$. A full numerical simulation of 1 would be necessary to accurately calculate the $\nu - \bar{\nu}$ asymmetry produced at its center and to optimize the setup's parameters.

In fig. 10 we show the results of this averaging for the $C\nu B$ asymmetry and the corresponding gradient around the center of our proposed setup for the three sets of parameters of table 2. Fig. 10 also shows the produced asymmetry for different neutrino flavors. Notice that an excess of electron antineutrinos, is accompanied by an excess of muon and tau neutrinos. For our chosen benchmark values, even a 2 m depleted uranium structure provides an enhancement of more than 5 orders of magnitude to the $\nu - \bar{\nu}$ asymmetry relative to naive expectation in the Standard Model, and the corresponding gradient corresponds to an enhancement of $\mathcal{O}(30 - 100)$ when compared to the effect produced by the earth. Ultimately, a structure with $L = 100$ m provides for roughly an additional order of magnitude, when considering all neutrino flavors.

To conclude, we have shown that appropriately engineered structures of even $\mathcal{O}$(meter) in size have the potential to drastically alter the local $C\nu B$ distribution.

5 Detection Prospects

We have so far described how a structure like what is shown in fig. 1 is a diffraction grating for the $C\nu B$ that produces close to its center an asymmetry of size $\sim k\delta_\nu L$ and a gradient

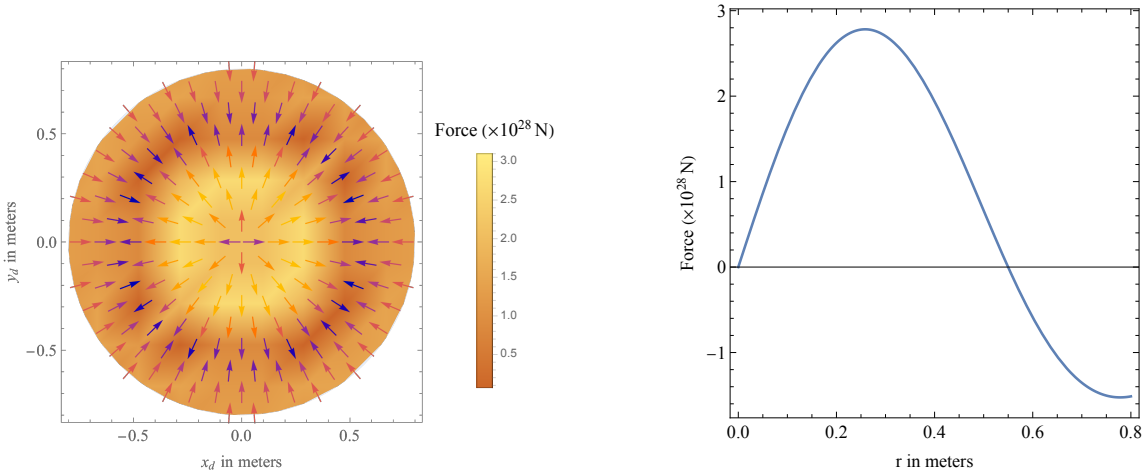

Figure 12. *On the left:* The force on a $(10\text{ cm})^3$ tungsten object produced around the center of grating 3 from table 2 for muon and tau neutrinos. *On the right:* The same force as a function of the distance from the center of the same grating.

of order the width w of the rods, orders of magnitude larger from those in the vacuum or near the Earth [3]. The next natural question to ask is whether the neutrino distribution induced can produce a detectable signal.

While in this paper we focus on manipulating the $C\nu B$ in a laboratory setting, we would like to provide a rough estimate for the benchmark of different detection methods. For concreteness we will consider two idealized setups that can detect the gradient force produced by our diffraction grating: a simple harmonic oscillator of frequency ω and a torsion balance similar to the one proposed in [7].

For both of these setups, the naive benchmark is the standard quantum limit (SQL). There are several strategies that are being explored on how this can be achieved, such as active feedback cooling of ultra-high Q resonators, but we will not commit to any such a strategy in this paper. The field of precision metrology is rapidly evolving in the last few decades and it is quickly pushing forward to the regime of quantum sensing (see for example [8]). For a harmonic oscillator the minimum detectable force is given by:

$$F_{SQL} = \sqrt{\frac{\hbar M \omega^2}{Q\ t_{int}}} \approx 3 \times 10^{-28}\ N \left(\frac{M}{19\ kg}\right)^{1/2} \left(\frac{\omega}{2\pi 0.1\text{ mHz}}\right) \left(\frac{10^8}{Q}\right)^{1/2} \left(\frac{3\text{ years}}{t_{int}}\right)^{1/2} \quad (5.1)$$

where t_{int} is the integration time of the experiment, Q is the quality factor, and M is the mass of the harmonic oscillator. In eq. 5.1 we have assumed that the harmonic oscillator is made out of a $(10\text{ cm})^3$ piece of Tungsten. For comparison, for the benchmark parameters used in sec. 4 we find a $C\nu B$ gradient induced force of $3 \times 10^{-28}\ N$ on a $(10\text{ cm})^3$ of Tungsten, which is comparable to the SQL of the force. The force field is shown in fig. 12. This is a force that is equivalence principle violating as it is material dependent. The corresponding acceleration is about 4 orders of magnitude larger than the one coming from neutrino coherent scattering [9–13].

It is worth pointing out that our diffraction grating can be mechanized and moved at frequencies much faster than the natural daily and annual modulation of the neutrino flux. These properties of the $C\nu B$ refractive force allow for valuable experimental handles in any effort to detect it.

Finally, we can extrapolate the parameters of current torsion balance experiments to the SQL to find:

$$\tau_{SQL} = \sqrt{\frac{2\hbar\kappa}{Q\ t_{int}}} \approx 8 \times 10^{-30}\ Nm \left(\frac{\kappa}{5.58\ \text{nJ/rad}}\right)^{1/2} \left(\frac{10^8}{Q}\right)^{1/2} \left(\frac{3\ \text{years}}{t_{int}}\right)^{1/2}, \quad (5.2)$$

where κ is the fibre torsional constant. For comparison, for the benchmark parameters used in sec. 4 and a lever arm of 10 cm we find a $C\nu B$ gradient induced torque of roughly $10^{-29}\ N \cdot m$ on a $(10\ \text{cm})^3$ of Tungsten, which is comparable to the SQL of the torque. While current experiments are far from these values, we can envisage future experiments striving to reach the quantum limit where the $C\nu B$ signal is detectable.

It is worth pointing out that laboratory scale structures can be mechanized, so that the neutrino signal can be manipulated at much shorter timescales compared to its natural daily and annual modulation. Such control is invaluable in designing a detection setup, as it provides another handle of control for the small signal. Yet another control results from the fact that the force is strongly material dependent. This is both a control parameter and a way to separately study the physics of electron, muon, and tau neutrinos in the early universe.

6 A diffraction grating for Dark Matter

Our proposed diffraction grating can be used to manipulate more than the $C\nu B$. Another obvious candidate is Dark Matter (DM). While we will not scan possible Dark Matter candidates in order to outline all possibilities, we find a very interesting benchmark: QCD axion DM with a decay constant f_a around $10^8 - 10^{10}$ GeV can be manipulated to produce a gradient force that is closer to what is currently being achieved in a laboratory setting than the $C\nu B$ gradient force. The index of refraction for the QCD axion arises through its quadratic coupling to nucleons (see for example [14]), which in the non-relativistic limit reduces to the following interaction potential in matter:

$$U_a \approx -\frac{\sigma_N}{8 m_a f_a^2} A\ n_{\text{matter}}, \quad (6.1)$$

where $\sigma_N \approx 60$ MeV, and n_{matter} is the number density of atoms with total number of nucleons A each. As the sign suggests, U_a is attractive and thus results in an index of refraction that is larger than unity by an amount:

$$\delta_a = -\langle \frac{m_a U_a}{k_a^2} \rangle = -\langle \frac{U_a}{m_a v_a^2} \rangle = \frac{A\sigma_N}{8 m_a^2 f_a^2} \langle v_a^{-2} \rangle n_{\text{matter}}, \quad (6.2)$$

where k_a and v_a are the axion momentum and velocity, respectively. Notice that for the QCD axion δ_a is independent of the axion decay constant f_a. Galactic DM follows a

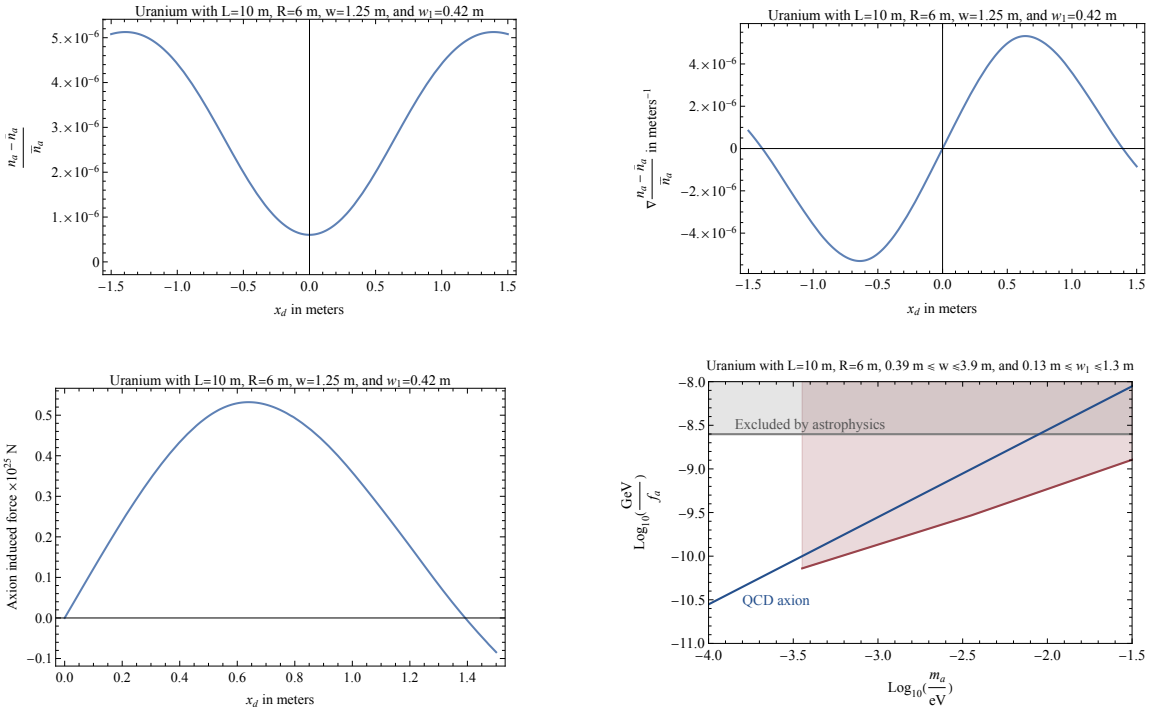

Figure 13. *Top left:* The axion density variation relative to the average galactic density. We assume the QCD axion with $f_a = 10^9$ GeV and a diffraction grating made out of Uranium for the parameters shown on the plot. *Top right:* The corresponding fractional density gradient. *Bottom left:* The force on a $(10\text{ cm})^3$ tungsten object produced around the center of the uranium grating with parameters shown on the plot for a QCD axion with $f_a = 10^9$ GeV. *Bottom right:* Assuming the same uranium diffraction grating, we show the reach in the general mass vs f_a plane. We also show the range excluded by astrophysics, as well as the line corresponding to the QCD axion mass and decay constant relation. We cutoff the calculated reach of the experiment at $f_a = 10^{10}$ GeV; for larger f_a the wavelength of the axion becomes larger than a few meters.

non-relativistic Maxwell-Boltzmann distribution, $\propto e^{-\frac{v_a^2}{\sigma_{\rm DM}^2}}$, with a velocity dispersion of $\sigma_{\rm DM} = 7.8 \times 10^{-4}$. Given this, we find that $\langle v_a^{-2}\rangle = (5.5 \times 10^{-4})^{-2}$. For iron this translates to $\delta_a = 2.8 \times 10^{-8}$, and for depleted uranium $\delta_a = 6.7 \times 10^{-8}$.

While the axion is its own antiparticle, this setup can still generate a local gradient in the axion density, and we can follow the procedure outlined in sections 3, and 4 to calculate the axion density and its corresponding gradient around the center of our diffraction grating. The axion mass is 5.7×10^{-3} eV$\frac{10^9\text{ GeV}}{f_a}$ and makes the deBroglie wavelength quite macroscopic with a value of $\lambda_a = 40$ cm$\frac{f_a}{10^9\text{ GeV}}$. This means that for a given grating radius R, the corresponding width of the rods has to be larger than the $C\nu B$ case, since $w \sim \sqrt{\lambda_a R}$. This is shown in fig. 13, where we present the generated QCD axion density, the corresponding gradient, and the force on a (10 cm^3) tungsten mass for a diffraction grating of size $L = 10$ m, and $R = 6$ m made out of depleted uranium. .For concreteness, we pick $f_a = 10^9$ GeV. We can see that, while the gradients are relatively small, the axion force benefits from the large axion density of 7×10^{10} cm$^3\frac{f_a}{10^9\text{ GeV}}$ to be much larger than

the $C\nu B$ generated one.

Assuming that the SQL calculated in section 5 can be reached, in fig. 13 we also present the corresponding forecast for an axion dark matter search. The reach of this setup falls within the traditional axion window and around the QCD axion f_a values that provide for the right DM abundance, when the PQ phase transition happens after the end of inflation [15, 16].

7 The stochastic force of the $C\nu B$ and the QCD axion

For completeness, it is worth comparing the results above to the force that naturally arises from the couplings above for both the relic neutrinos as well as the QCD axion due to fluctuations of the density at scales of order the deBroglie wavelength.

For the $C\nu B$, the force is stochastic in nature and fluctuates on $\mathcal{O}(\frac{1}{m_\nu v_\nu^2}) \sim$ ns time scales. It is coherent on objects of size $\lambda_{dB} \approx 2$ mm and produces an acceleration on Tungsten of size:

$$a_{\nu-\text{stoch}} \approx \frac{G_F(A-Z)}{2\sqrt{2}m_{\text{tungsten}}}\nabla n_\nu \sim 3\times 10^{-22}\frac{m}{s^2}, \tag{7.1}$$

where m_{tungsten} is the mass of the tungsten atom. This is naively larger than the acceleration of roughly $10^{-29}\ \frac{m}{s^2}$ calculated in sec. 5. The latter though is a coherent acceleration component, since our proposed diffraction grating produces a modulation of the time-averaged $\nu-\bar{\nu}$ asymmetry. This means that the sensitivity of any experiment to this acceleration will continue to improve as $t_{int}^{-1/2}$ even for years-long integration time, while mechanization of the diffraction grating can provide for an additional control parameter that can modulate the signal at a chosen frequency, thus making the effect presented in sec. 5 a worthwhile target.

Similarly, for the QCD with f_a around 10^9 GeV, any atom will experience an acceleration produced by the gradient set by the axion deBroglie wavelength of size:

$$a_{a-\text{stoch}} \approx \frac{\sigma_N}{8m_a f_a^2}\nabla n_a \sim 2\times 10^{-21}\frac{m}{s^2}\left(\frac{10^9\ \text{GeV}}{f_a}\right) \tag{7.2}$$

The QCD axion DM induced force is qualitatively different from the $C\nu B$ one. The corresponding acceleration $a_{a-\text{stoch}}$ has an oscillatory component with the frequency that is twice that set by the mass, i.e. $2\omega_a = 2\pi(2\ \text{THz})\left(\frac{10^9\ \text{GeV}}{f_a}\right)$, and it is coherent for roughly $\mathcal{O}((m_a v_a^2)^{-1}) \sim \mu s\left(\frac{10^9\ \text{GeV}}{f_a}\right)^{-1}$ time scales. $a_{a-\text{stoch}}$ also has a component analogous to $a_{\nu-\text{stoch}}$: it varies over time scales of $\mathcal{O}((m_a v_a^2)^{-1})$ and it is coherent for a similar amount of time. Its magnitude is the same as the oscillatory part of $a_{a-\text{stoch}}$.

The time-averaged axion density modulation that the setup of fig 1 produces and was calculated in sec. 6, results in an acceleration of $\sim 10^{-26}\ \frac{m}{s^2}\left(\frac{10^9\ \text{GeV}}{f_a}\right)^{1/2}$, which is again much smaller than the one of eq. 7.2. The frequency associated with $a_{a-\text{stoch}}$ for a QCD

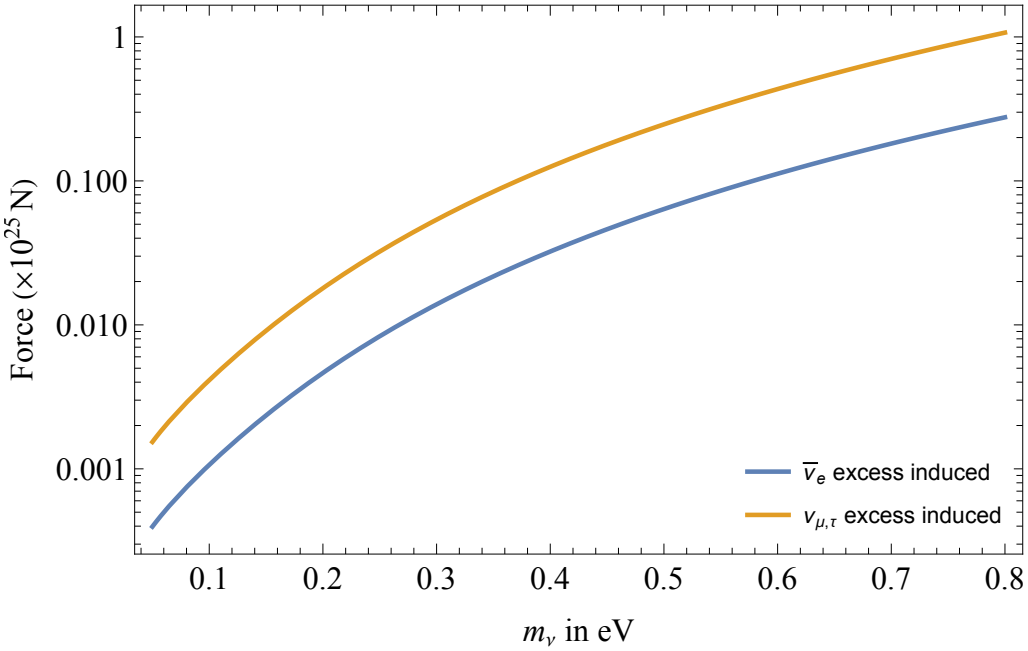

Figure 14. The maximum induced force on a $(10\text{ cm})^3$ tungsten mass from the neutrino asymmetry gradient produced by grating 3 of table 2 as a function of the heaviest neutrino mass. This includes possible enhancements in the density due to clumping as calculated in [17–20].

axion in the range of 10^8 GeV $\leq f_a \leq 10^{10}$ GeV is prohibitevely high for any reasonable accelerometer, as these frequencies correspond to molecular vibrational and rotational excitation modes. In contrast, the effect described in sec. 6 can result to an extremely low frequency signal with the possibility of long integration times, when the DM phase grating is mechanized.

8 Discussion

In this paper we have presented an engineered structure of reasonable size that can be used to manipulate the $C\nu B$ and DM distributions in a laboratory scale. Throughout we have set the neutrino mass to 0.1 eV and the size of the asymmetry as well as force scale linearly with it. For heavier neutrinos, the effects of clumping in the cluster could be significant [17–20]. These are included in fig. 14, which shows the maximum force induced by grating 3 of table 2 as a function of the neutrino mass and depending on the neutrino flavor. If one ignores the cosmological bounds, and assumes that the maximum allowed neutrino mass is optimistically 0.8 eV [21], the neutrino produced force can be 10^{-25} N, which is comfortably above the quantum limit calculated in section 5.

Our estimates are for Dirac neutrinos and ignore the effects of the neutrinos being in mass eigenstates instead of flavor, which we do not expect to be more than $\mathcal{O}(1)$. We will present the Majorana case in an upcoming work [22].

Superficially our set-up seems analogous to lenses, which compress and enhance the density of photons in specific locations - focal points. This is misleading, as the physics

of neutrinos and photons are very different. First, photons are bosons where as the $C\nu B$ neutrinos are fermions that are not that far from being maximally packed, so they cannot be significantly focused or compressed. In addition, focusing of black body omnidirectional radiation in the geometric optics approximation, as is the case for lenses, is constrained by the conservation of the etendue or Liouville's theorem and has to make use of the relative motion of the Earth to the $C\nu B$ in order to have a non-zero effect. Furthermore previous discussions relying on geometric optics [23] and Bragg reflection [24] required multi-km^3 structures.

Our setup circumvents these issues because it does not rely on geometric optics, it is diffractive in nature. The rods, instead of focusing the neutrinos, separate them by creating a carefully designed region of non-zero chemical potential, just as an electric field can create charge separation in a thermal plasma. This, in combination with the fact that we rely on diffraction, i.e. the wave nature of neutrinos, allows us to avoid the constraints of etendue conservation and propose structures much smaller than the multi-km^3 structures proposed before.

After the Cabibbo-Langacker "no-go" theorem of 1982, the Stodolsky effect [25] was believed to be the only non-zero effect of $\mathcal{O}(G_F)$. Our setup enhances this effect by $\sim 4\times10^6$ relative to the naive SM expectation, nevertheless the Stodolsky effect is now dwarfed by the gradient force. This is because the gradient force gets a boost by the atomic number ($\mathcal{O}(100)$) and does not suffer from the relative velocity suppression of $v \sim 10^{-3}$ that the Stodolsky effect has to rely on. For completeness, we estimate the Stodolsky torque on a $(10\text{ cm})^3$ piece of spin-polarized iron to be $\sim 10^{-33} N \cdot m$ for a neutrino mass of 0.1 eV. As discussed in sec. 5, proposals for forces relying on coherent scattering result in forces that are $\mathcal{O}(10^4)$ times smaller than the forces proposed here.

In this paper, we set an experimental target for $C\nu B$ searches by factorizing the observation of the $C\nu B$ to manipulation and detection. Our proposed setup for manipulation is the first of its kind and its simplicity suggests that there could be several opportunities for improvement.

Acknowledgments

We would like to thank Giorgio Gratta and Andy Geraci for very valuable conversations. We also thank Masha Baryakhtar, Matheus Hostert, Marios Galanis, and Junwu Huang for useful discussion during the completion of this work. AA is grateful to John Arvanitakis for help with numerical calculations. AA is also thankful for the support of the Stavros Niarchos Foundation and the Gordon and Betty Moore foundation. SD is grateful for support from the National Science Foundation under Grant No. PHYS-2014215, and from the Gordon and Betty Moore Foundation Grant GBMF7946. Research at Perimeter Institute is supported in part by the Government of Canada through the Department of Innovation, Science and Economic Development Canada and by the Province of Ontario through the Ministry of Colleges and Universities.

References

[1] N. Cabibbo and L. Maiani. *Phys. Lett. B*, 114:115–117, 1982. doi: 10.1016/0370-2693(82)90127-7.

[2] Paul Langacker, Jacques P. Leveille, and Jon Sheiman. *Phys. Rev. D*, 27:1228, 1983. doi: 10.1103/PhysRevD.27.1228.

[3] Asimina Arvanitaki and Savas Dimopoulos. URL https://arxiv.org/abs/2212.00036. [arXiv:2212.00036 [hep-ph]].

[4] Anatoly Snigirev, Victor Kohn, Irina Snigireva, and Bruno Lengeler. *Nature*, 384(6604): 49–51, 1996.

[5] A Snigirev, V Kohn, I Snigireva, A Souvorov, and B Lengeler. *Applied optics*, 37(4):653–662, 1998.

[6] Max Born and Emil Wolf. *Principles of optics: electromagnetic theory of propagation, interference and diffraction of light*. Elsevier, 2013.

[7] E. A. Shaw, M. P. Ross, C. A. Hagedorn, E. G. Adelberger, and J. H. Gundlach. *Physical Review D*, 105(4), feb 2022. doi: 10.1103/physrevd.105.042007. URL https://doi.org/10.1103%2Fphysrevd.105.042007.

[8] Markus Aspelmeyer, Tobias J. Kippenberg, and Florian Marquardt. *Rev. Mod. Phys.*, 86: 1391, 2014. doi: 10.1103/RevModPhys.86.1391.

[9] B. F. Shvartsman, V. B. Braginsky, S. S. Gershtein, Ya. B. Zeldovich, and M. Yu. Khlopov. *JETP Lett.*, 36:277–279, 1982.

[10] Gintaras Duda, Graciela Gelmini, and Shmuel Nussinov. *Phys. Rev. D*, 64:122001, 2001. doi: 10.1103/PhysRevD.64.122001.

[11] Valerie Domcke and Martin Spinrath. *JCAP*, 06:055, 2017. doi: 10.1088/1475-7516/2017/06/055.

[12] Jack D. Shergold. *JCAP*, 11(11):052, 2021. doi: 10.1088/1475-7516/2021/11/052.

[13] Martin Bauer and Jack D. Shergold. *JCAP*, 01:003, 2023. doi: 10.1088/1475-7516/2023/01/003.

[14] Anson Hook and Junwu Huang. *JHEP*, 06:036, 2018. doi: 10.1007/JHEP06(2018)036.

[15] Marco Gorghetto, Edward Hardy, and Giovanni Villadoro. *SciPost Phys.*, 10(2):050, 2021. doi: 10.21468/SciPostPhys.10.2.050.

[16] Malte Buschmann, Joshua W. Foster, Anson Hook, Adam Peterson, Don E. Willcox, Weiqun Zhang, and Benjamin R. Safdi. *Nature Commun.*, 13(1):1049, 2022. doi: 10.1038/s41467-022-28669-y.

[17] Andreas Ringwald and Yvonne Y. Y. Wong. Gravitational clustering of relic neutrinos and implications for their detection. *JCAP*, 12:005, 2004. doi: 10.1088/1475-7516/2004/12/005.

[18] P. F. de Salas, S. Gariazzo, J. Lesgourgues, and S. Pastor. Calculation of the local density of relic neutrinos. *JCAP*, 09:034, 2017. doi: 10.1088/1475-7516/2017/09/034.

[19] Jue Zhang and Xin Zhang. Gravitational clustering of cosmic relic neutrinos in the Milky Way. *Nature Commun.*, 9:1833, 2018. doi: 10.1038/s41467-018-04264-y.

[20] P. Mertsch, G. Parimbelli, P. F. de Salas, S. Gariazzo, J. Lesgourgues, and S. Pastor. Neutrino clustering in the Milky Way and beyond. *JCAP*, 01:015, 2020. doi: 10.1088/1475-7516/2020/01/015.

[21] Ivan Esteban, M. C. Gonzalez-Garcia, Michele Maltoni, Thomas Schwetz, and Albert Zhou. *JHEP*, 09:178, 2020. doi: 10.1007/JHEP09(2020)178.

[22] A. Arvanitaki, S. Dimopoulos, M. Galanis, and O. Simon. to appear.

[23] C. C. Speake and J. Leon. *Class. Quant. Grav.*, 13:A207–A217, 1996. doi: 10.1088/0264-9381/13/11A/030.

[24] P. F. Smith and J. D. Lewin. *Acta Phys. Polon. B*, 15:1201–1214, 1984.

[25] Leo Stodolsky. *Phys. Rev. Lett.*, 34:110, 1975. doi: 10.1103/PhysRevLett.34.110. [Erratum: Phys.Rev.Lett. 34, 508 (1975)].